Characterizing Nonlinear Field Dependent Conductivity Layers to Mitigate Electric Field Within (U)WBG Power Modules Under High Frequency, High Slew Rate Square Voltage Pulses

Pujan Adhikari and Mona Ghassemi

Zero Emission, Realization of Optimized Energy Systems (ZEROES) Laboratory

Department of Electrical and Computer Engineering

The University of Texas at Dallas

Richardson, TX, USA

pujan.adhikari@utdallas.edu, mona.ghassemi@utdallas.edu

Abstract—A vast majority of research on (U)WBG power modules has been going on to implement nonlinear resistive field grading material on metal-brazed substrates in reducing the electric field that is maximum at triple points (TPs). However, nearly all investigations have been conducted under either DC or 50/60 Hz sinusoidal AC voltages, even though the actual operation of envisioned (U)WBG power modules involves high-frequency square voltages with high slew rates. It has been validated by several studies that fast rise times of square voltages rapidly degrade the breakdown strength of insulation materials, leading to premature failure. Therefore, this paper introduces a nonlinear resistive field grading material or field-dependent conductivity (FDC) layer around the TP and metal edges to evaluate the electric field mitigation under a high frequency and high slew rate square voltage. The modeling and simulation of both coated and uncoated (U)WBG substrates were performed in COMSOL Multiphysics to assess the electric field reduction with the nonlinear FDC layer. The improvement of reduction in electric field under 100 kHz high slew rate square voltage is compared with that of 60 Hz. The results reveal a significant decrease in field stress at the TP, even under square voltages with fast rise times and high frequencies, when applying a nonlinear FDC coating, as opposed to the uncoated substrate. The influence of switching field (Eb) and nonlinearity coefficient (a) of nonlinear FDC layer is studied under 100 kHz square voltage, and it is concluded that a and Eb should be more than 10 and less than 8 kV/mm, respectively to achieve effective performance of resistive field grading material.

Keywords— (U)WBG power modules, high frequency, high slew rate, nonlinear field grading material, triple points, electric field reduction, packaging

I. INTRODUCTION

As the world leans towards greater electrification and clean energy in pursuit of net-zero emissions, the daily surge in demand for electrical power becomes inevitable. Addressing this escalating need involves a strategic elevation in voltage. Simultaneously, there's a growing inclination to reduce the weight and size of power electronics modules. The convergence of these two notions gives rise to the innovative concept of high-voltage, high-power-density engineering [1].

Operating power modules at high voltage and power density revolves around adopting wide bandgap (WBG) materials such as SiC and GaN and ultra-wide bandgap (UWBG) materials like diamond, AlN, and h-BN [2]. (U)WBG materials exhibit higher blocking voltages compared to traditional Si-based devices, with a noteworthy advantage being their suitability for operation under higher slew rates (dv/dt) and higher frequency voltage pulses. However, high slew rate and high frequency are the two most crucial specifications affecting insulation systems' performance [3].

A power electronics module has two key insulation components: the ceramic substrate, which isolates the chips and removes heat, and the encapsulation materials, shielding the semiconductors, connections and substrate from vibrations, dirt and moisture [4, 5]. While (U)WBG power electronics modules excel in operating at high frequency and slew rates, the insulation materials within the modules face a challenge as they endure these parameters beyond their normal limits, heightening the risk of insulation damage. Additionally, protrusions are created around substrate and metal edges during power module packaging, and triple points (TPs) are formed at the junction of metallization layers, ceramic substrate, and encapsulation materials. It has been validated through several studies that the electric field surpasses the withstand limit at these junctions and is responsible for the initiation of partial discharges (PDs) and insulation failure [6-11].

To tackle this issue of the high electric field at TP, various mitigation strategies have been proposed, which can be basically categorized as: (1) geometrical techniques, (2) field grading materials, and (3) alternative encapsulants [12-17]. Geometrical techniques are less effective when mitigating field stress independently and come with some consequences. For example, increasing metal layer offset and ceramic thickness creates thermal management issues while introducing protruding substrate alone isn't enough to bring down field stress values to criterion limits. Alternatives for silicone gel as an encapsulation material aren't mature enough, as additional investigations on thermal stress must be carried out. Field

This work was partially funded by the U.S. National Science Foundation (NSF) under Award 2306093.

grading materials, especially resistive field grading materials, have proven to be the best strategy for resolving high electric field issues [18-21]. However, almost all the research have evaluated the efficacy of resistive field grading materials or nonlinear field-dependent conductivity (FDC) layers for DC and power frequency sinusoidal AC voltages. As the envisaged (U)WBG modules will operate under high-frequency square voltages with fast rise times, these investigations might not be able to predict their actual capability. Additionally, studies have validated that the PD behavior of (U)WBG power modules is different and more severe when operated under high slew rate square wave voltages [22]. Therefore, this paper assesses the efficacy of the nonlinear FDC layer in electric field mitigation around TPs for a 25 kV power module under a high slew rate square voltage with frequencies up to 100 kHz.

II. GEOMETRY FOR FEM ANALYSIS

The active metal brazing (AMB) substrate shown in Fig 1. is a well-established (U)WBG power module packaging technique. In this technique, both the upper and ground metal electrodes are brazed to the ceramic substrate (AlN in our case). The soldering of the IGBT/diode and baseplate onto the metalized ceramic substrate cannot be done without defects, and thus, small protrusions are introduced on metal edges on top of the substrate [23]. Triple points (TPs) are formed at the junction of metallization layers, ceramic substrate, and encapsulation material, and previous studies have shown that the electric field value is the highest at these junctions.

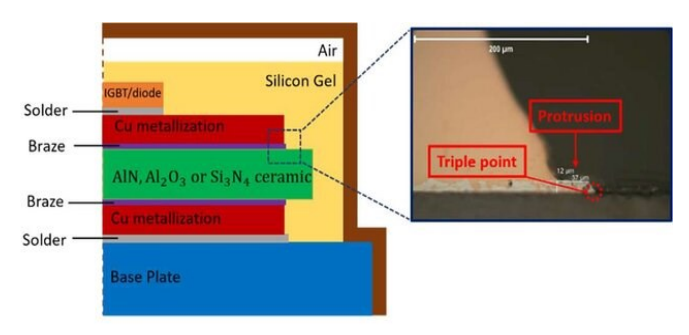


Fig. 1. Schematic diagram of an IGBT/diode with AMB substrate showing protrusion and triple point.

The best way to study the high voltage and high-frequency effect of (U)WBG power modules on the electric field at TPs is by performing finite element method (FEM) examination. In this investigation, COMSOL Multiphysics has been used to simulate the electric field distribution for all cases. To estimate field calculation correctly, the dimensions of the model and the associated properties of insulation materials are taken to be in accordance with the actual (U)WBG module packaging. Fig. 2 illustrates the geometry of the base case considered for simulation. Both metallization layers, which are 292 µm thick, are soldered to an AlN substrate and encapsulated by silicone gel (SG). The dielectric breakdown strength of the AlN substrate is found between 20-30 kV/mm for different manufacturers [24], and it is 25 kV/mm in this paper. The electrical conductivities of AlN substrate and SG are 10⁻¹¹ and 10⁻¹³, respectively, and their relative permittivity is assumed to be 9 and 2.86, respectively. The protrusion on the substrate, shown in Fig.1, is created having 12 μm height and 37 μm length.

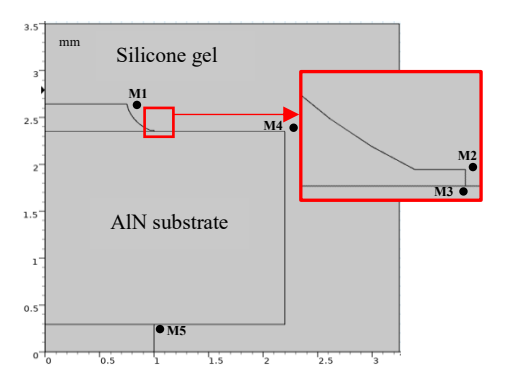


Fig. 2. The geometry considered for the base case in COMSOL Multiphysics simulations.

IEC 61287-1 states that power modules must meet the oneminute insulation test requirement with AC voltage of V_{rms} = $(2U_b/\sqrt{2+1})$ kV, where U_b is the module's blocking voltage [18]. For our module with 25 kV blocking voltage, $V_{max} = 51.41$ kV. Thus, a 51.41/25 =2.06 thickness is chosen for the AlN substrate. IEC 61287-1 specifies a one-minute application of the AC voltage at 50/60 Hz, reaching a maximum of $1.5U_b$, followed by a 30-second application at $1.1U_b$. During the last 30 seconds of this test, the recorded PD level must not exceed 10 pC. So, in this paper, a voltage of $1.1U_b = 27.5$ kV is employed to the top metal electrode, whereas the bottom metal electrode is grounded to create the same conditions as the actual PD measurement test. Even though the IEC 61287-1 criterion is for power frequency sinusoidal AC voltage, since there is no standard available for high-frequency square waveform [22], we used the same criterion for our electric field analysis.

Five measuring points, which are $15 \mu m$ away from the metallization edges, are taken to eliminate the field dependency on mesh size while calculating the electric field values in the base model case. Fig. 2. shows these points (M1, M2, M3, M4, and M5) at different locations within the model.

III. SIMULATION RESULT FOR BASE MODEL UNDER 60 HZ SQUARE VOLTAGE

As the base case scenario for this paper, the model shown in Fig. 2 is simulated under a 60 Hz square voltage waveform. The electric field distribution plot under 60 Hz, 27.5 kV square voltage is shown in Fig. 3, which is obtained from COMSOL Multiphysics.

Table I shows the values of electric field intensity at five predefined measurement points for the base case under 60 Hz square voltage. As seen from the table, the electric field values at M2, M3 (15 μm away from the TP at the upper electrode), and M5 (15 μm away from the TP at the ground electrode) are significantly higher than the breakdown strength of the ceramic substrate (AlN) and encapsulant (SG). Therefore, to bring the electric field at TPs to the acceptable limits, nonlinear FDC layers are introduced in subsequent sections.

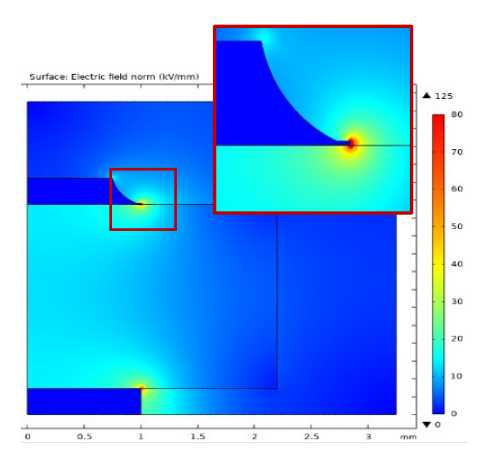


Fig. 3. Electric field distribution showing maximum field stress at TPs under 60 Hz square voltage.

Table I. E value (kV/mm) at M1-M5 for section III

| Measuring points | M1 | M2 | M3 | M4 | M5 |
|------------------------|-------|-------|-------|------|-------|
| Electric field (kV/mm) | 15.51 | 53.54 | 49.94 | 2.86 | 44.55 |

IV. MODELING AND SIMULATION FOR NONLINEAR FIELD-DEPENDENT CONDUCTIVITY (FDC) LAYER

Nonlinear FDC layers are prepared by incorporating high-conductivity filler particles (e.g., ZnO microvaristor) in a polymer matrix (silicone gel in our case) [25]. The field-dependent feature of these coatings allows uniform field distribution within (U)WBG power modules by allowing conductivity values to rise in high electric field areas such as TPs when electric field (E) becomes higher than switching field (E_b). The relationship between nonlinear FDC layer's conductivity and electric field is given by:

$$\sigma(E) = \sigma_0(1 + (E/E_b)^{\alpha - 1})$$
 (1)

As seen from the above equation, the performance of these coatings mainly depends upon two parameters: nonlinearity coefficient (α) and switching field (E_b). Previous studies have shown that α must be higher than 10 to achieve frequency-independent behavior and E_b should be equal to the applied voltage divided by layer length [18, 24]. In subsequent sections, we investigate how effective the nonlinear FDC layers are on electric field mitigation at different frequencies of square voltage.

A. Nonbridging Nonlinear FDC Layer

In this section, we implement the nonlinear FDC layer around the TP of the HV electrode, as depicted in Fig. 4. The FDC layer is considered to have 100 μ m thickness, and it is designed to cover the points M2, M3, and their surrounding regions in both AlN substrate and silicone gel. Two additional points, M6 and M7, are considered to evaluate the electric field just below the FDC layer on the AlN substrate and just above the FDC layer on SG when the nonlinear FDC coating is introduced. The values of α and E_b are assumed to be 12 and 4 kV/mm, respectively, and the low field conductivity (σ_0) is 3.3×10^{-11} S/m, as we used ZnO microvaristor as a high conductivity filler material in our study.

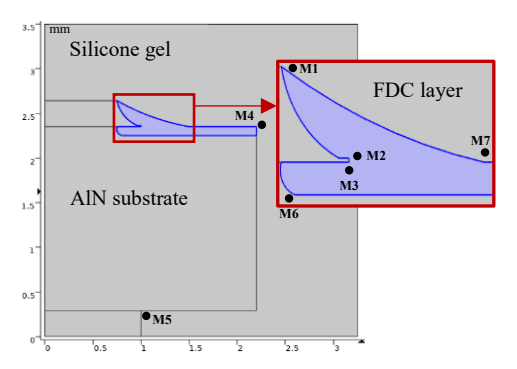


Fig. 4. Nonlinear nonbridging FDC coating applied to the protrusion and TP regions at the HV electrode.

The electric field distribution for this case obtained from COMSOL Multiphysics is illustrated in Fig. 5, and it's seen that, although the electric field at points M1 and M2 are reduced, the maximum field is now concentrated at point M5 of the ground electrode.

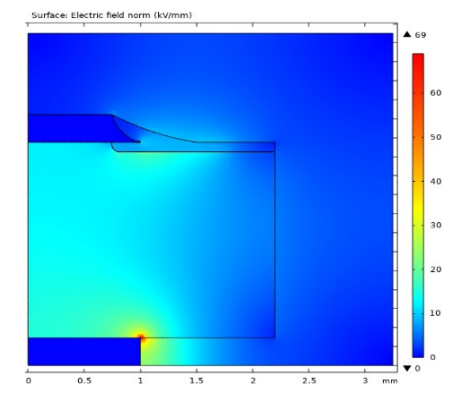


Fig. 5. Electric field distribution for a nonlinear nonbridging FDC layer showing high electric field at TP of the ground electrode.

As we can observe from Table II, although the nonbridging nonlinear FDC coating reduced the field stress at M2 and M3 by 82% and 81.5%, respectively, the maximum electric field is now seen at point M5, which considerably exceeds the criterion threshold of 25 kV/mm. This can be elucidated by the fact that the field stress gets shifted from the HV electrode to the ground electrode areas because of implementing FDC coatings on the HV electrode. Thus, we can conclude that the nonbridging nonlinear FDC layer isn't enough to solve the electric field stress issue in (U)WBG power modules. So, we introduce a bridging FDC layer in the next section.

Table II. E value (kV/mm) at M1-M7 for section IV-A

| Measuring points | M1 | M2 | M3 | M4 | M5 | M6 | M7 |
|------------------------|------|------|------|------|-------|-------|------|
| Electric field (kV/mm) | 5.80 | 9.61 | 9.06 | 2.90 | 50.42 | 16.49 | 9.44 |

B. Bridging Nonlinear FDC Layer

In this section, we apply a nonlinear FDC layer that bridges the HV and the ground electrode. All the parameters of the coating are similar to the previous case. As shown in Fig. 6, the same thickness of 100 μm is used for the FDC layer, and the thickness of the coating becomes 292 μm while bridging the

HV metallization layer to the ground metallization layer at the end.

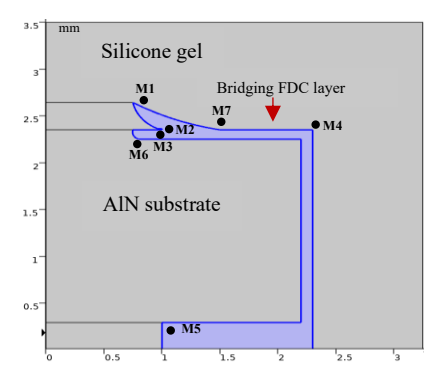


Fig. 6. Nonlinear FDC coating bridging the HV and ground electrodes.

Table III summarizes the electric field at 7 measuring points (M1-M7) when a bridging nonlinear FDC layer, shown in Fig. 6, is applied. The electric field reduction across all regions within the power module can also be seen from the electric field distribution obtained from COMSOL Multiphysics, as shown in Fig. 7.

Table III. E value (kV/mm) at M1-M7 for section IV-B

| Measuring points | M1 | M2 | M3 | M4 | M5 | M6 | M7 |
|------------------|------|------|------|------|------|-------|------|
| Electric field | 6.52 | 0.06 | 0.22 | 4.04 | 0.27 | 18.81 | 0.64 |
| (kV/mm) | 0.55 | 9.90 | 9.23 | 4.04 | 9.27 | 10.01 | 9.04 |

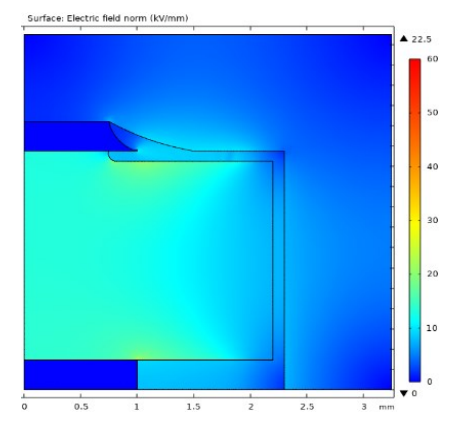


Fig. 7. Electric field distribution for a bridging nonlinear FDC coating under 60 Hz square voltage

As depicted in Table III, the electric field at point M5 of the ground electrode decreased by 81.6% with the introduction of bridging nonlinear FDC coating. The maximum field stress of 18.81 kV/mm is now seen at point M6 (right below the FDC layer in the AlN substrate), which is still lower than our 25 kV/mm limit. Therefore, it can be concluded that electric field mitigation can be achieved with nonlinear FDC coating for power frequency square voltage pulses.

V. SIMULATION RESULTS FOR NONLINEAR FDC LAYER UNDER HIGH FREQUENCY AND HIGH SLEW RATE SQUARE VOLTAGE

In section IV-B, a bridging nonlinear FDC coating achieved electric field mitigation under 60 Hz square voltage pulses. But,

as the envisioned (U)WBG power modules will operate under high slew rate square voltages with high frequencies (100 kHz and more), the effectiveness of the coating must be studied under those conditions [1]. In this section, high slew rate square pulses with 4 different frequencies of 1 kHz, 10 kHz, 50 kHz, and 100 kHz are applied, and the electric field values at those 7 measuring points are compared with 60 Hz square voltage. The FDC layer's thickness and properties are the same as before.

Table IV. E value (kV/mm) at M1-M7 for Section V

| Points/ Frequency | M1 | M2 | M3 | M4 | M5 | M6 | M7 |
|----------------------|------|-------|-------|------|-------|-------|-------|
| 1 kHz | 7.40 | 11.32 | 12.87 | 3.39 | 11.71 | 17.41 | 12.35 |
| 10 kHz | 7.99 | 13.43 | 14.15 | 3.20 | 14.03 | 16.22 | 12.72 |
| 50 kHz | 8.35 | 14.97 | 16.07 | 3.14 | 15.91 | 15.98 | 11.24 |
| 100 kHz | 8.51 | 15.92 | 17.16 | 3.13 | 17.00 | 16.07 | 10.92 |

As presented in Table IV, implementing a nonlinear FDC layer works well even for high frequencies of 100 kHz and more. The maximum electric field at point M3 is 17.16 kV/mm, which is still within the criterion limit of 25 kV/mm by 31%. So, it can be concluded that a bridging nonlinear FDC coating can be applied to protrusion and TPs within (U)WBG power modules for mitigating electric field stress under high slew rate high-frequency square voltages.

As mentioned before, the switching field (E_b) and nonlinearity coefficient (α) are the two most important parameters determining the properties of nonlinear FDC coatings. So, in subsequent subsections, we study the influence of these two variables on the electric field mitigation under 100 kHz square voltages.

A. Effect of Nonlinearity Coefficient (α)

Previous investigations have shown that α has a negligible impact on the performance of nonlinear FDC coating for DC voltage but significantly affects power frequency sinusoidal AC voltage [26]. In this subsection, we study the efficiency of implementing the nonlinear FDC layer in electric field mitigation at TPs by observing the effect of α . The value of α is increased from 8 to 16 to study the influence.

Fig. 8 depicts how α influences the values of electric field at predefined measurement points for 100 kHz high slew rate square voltage. As we can see from the figure, the electric field at all measurement points keeps on decreasing if we raise the value of α. For example, the electric field at M2, M3, and M5 is reduced by 45%, 42%, and 44%, respectively, when α is increased from 10 to 16. However, a higher value of α than this leads to larger computation time. It should be noted that once we decrease α to be lower than 10 (i.e., 8 in our study), the electric field at all three points, M2, M3, and M5, increases beyond the criterion limit (25 kV/mm). The electric field is increased by 27%, 38%, and 22%, respectively when α is reduced from 10 to 8. This is expected as it was explained earlier that the frequency- independent performance of nonlinear FDC layer can be achieved only when the value of the nonlinearity coefficient (α) is equal to or more than 10.

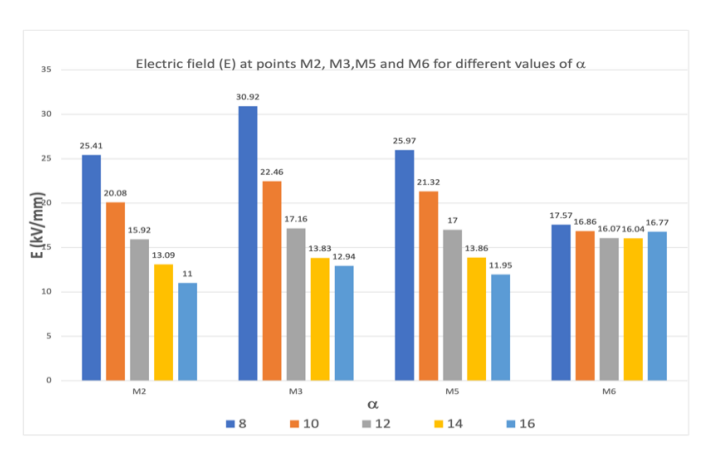


Fig. 8. The electric field at M2, M3, M5, and M6 for various values of nonlinearity coefficient (α) of nonlinear FDC layer.

B. Effect of Switching Field (E_b)

Fig. 9. summarizes the influence of E_b on electric field reduction with a nonlinear FDC layer under 100 kHz high slew rate square voltage. This is of particular importance as the layer achieves a nonlinear conductivity feature once E becomes higher than E_b, allowing the conduction of current by an increase in the layer's conductivity. As seen from Fig. 9, lowering the value of E_b helps in electric field mitigation at points M2 (SG), M3 (AlN substrate), and M5 (TP at ground electrode). Still, once reaching a specific value, the electric field value at measuring point M6 (right below the FDC coating on the upper electrode) starts to increase considerably. Also, increasing E_b beyond 8 kV/mm negatively influences field reduction under 100 kHz square wave voltage, as the electric field exceeds 25 kV/mm. The electric field values at points M2, M3, and M5 increase by 77%, 92%, and 74%, respectively, when we change E_b from 4 kV/mm to 8 kV/mm. The lowest maximum electric field occurs when $E_b = 4 \text{ kV/mm}$, which is 16.043 kV/mm at point M6.

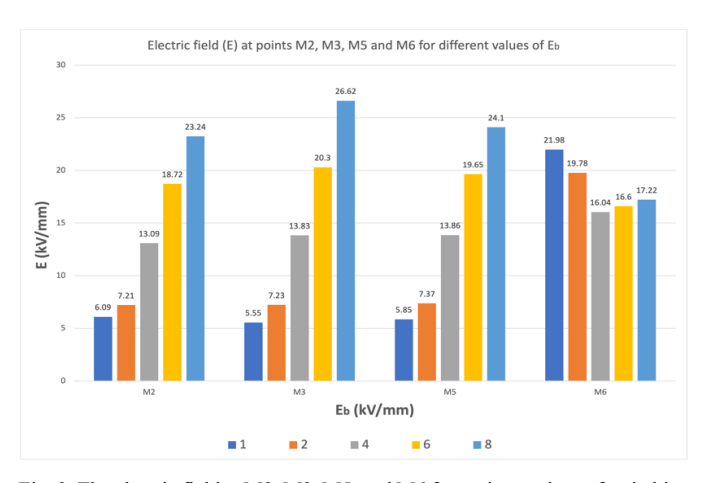


Fig. 9. The electric field at M2, M3, M5, and M6 for various values of switching field (E_b) of nonlinear FDC layer.

Different points that are taken within the nonlinear FDC layer possess their own specific values of σ , as E is dependent upon the geometry, resulting in distinct values at separate points within the geometry and the value of E depends on σ as well.

This nonlinear and complex relationship of E and σ in the nonlinear FDC layer affects the values of E within the AlN substrate and SG which is a difficult phenomenon to explain. But it's clear from the above simulations that increasing α of the nonlinear FDC layer has a positive impact on electric field mitigation.

C. Comparison of Electric Field Reduction with Nonlinear FDC Layer under 60 Hz, and 100 kHz Square Voltage

Fig. 10. illustrates the electric field at points M2, M3, M5, and M6 for a nonlinear FDC coating having 5 switching field (E_b) values under 60 Hz square voltage. As shown in Fig. 10, the electric field values at these points keep increasing if we increase E_b . Compared to the electric field under high-frequency (100 kHz) square voltage, which was more than the criterion limit when E_b was increased higher than 8 kV/mm, the nonlinear FDC coating works well for higher E_b values (14 kV/mm) when (U)WBG power modules are under power frequency. So, it's obvious to conclude that (U)WBG power modules will have higher electric field stress under high-frequency, high slew rate square wave voltage, and attention must be driven to study electric field mitigation strategy in this case. Fig. 11 shows electric field distribution with α =12 and E_b = 4 kV/mm for 100 kHz high slew rate square voltage.

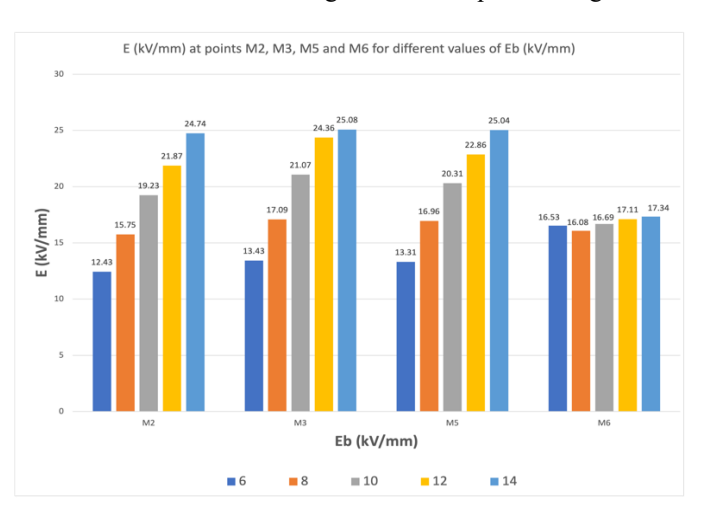


Fig. 10. The electric field values at M2, M3, M5, and M6 for nonlinear FDC layer with α =12 and different E_b under 60 Hz square voltage.

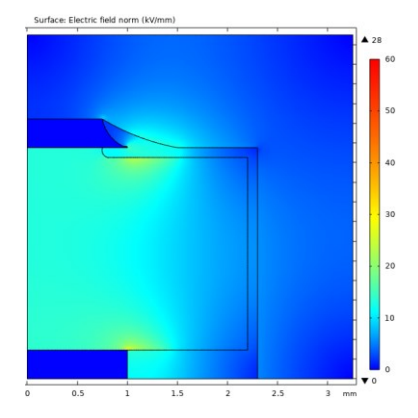


Fig. 11. Electric field distribution for nonlinear FDC layer with α =12 and E_b = 4 kV/mm for 100 kHz high slew rate square voltage.

VI. CONCLUSION

With the research on (U)WBG power modules rapidly advancing, significant attention needs to be dedicated to insulation systems within these modules as they limit their optimal capability. However, only a few papers deal with the high electric field stress challenge in insulation systems within modules under real-world situations of square voltage pulses. This paper investigated the efficacy of a nonlinear fielddependent conductivity (FDC) layer under high-frequency and high slew rate square voltages. It is observed that the electric field issue at TPs is more critical under high-frequency square voltage compared to the power frequency case. However, the electric field at TPs can be significantly reduced with the introduction of nonlinear field grading material. It is seen that a field reduction of 70%, 65%, and 62% on silicone gel, AlN substrate, and ground electrode can be achieved with a bridging nonlinear FDC layer around protrusions and TPs under 100 kHz fast rise square voltage. Additionally, it is suggested that the performance of the FDC layer depends upon E_b and α parameters. To achieve optimal performance, the value of α should be more than 10, and E_b should be lower. Finally, as shown in Fig. 11., with α and E_b being 14 and 4 kV/mm, respectively, the maximum mitigation on the electric field intensity at all considered points around TPs is obtained.

VII. REFERENCES

- [1] B. Zhang, M. Ghassemi, and Y. Zhang, "Insulation Materials and Systems for Power Electronics Modules: A Review Identifying Challenges and Future Research Needs," *IEEE Trans. Dielectr. Electr. Insul.*, vol. 28, no. 1, pp. 290–302, Feb. 2021.
- [2] Y. Chen, A. Iradukunda, H. A. Mantooth, Z. Chen, and D. Huitink, "A Tutorial on High-Density Power Module Packaging," *IEEE J. Emerg. Sel. Top. Power Electron.*, vol. 11, no. 3, pp. 2469–2486, Jun. 2023.
- [3] M. Ghassemi, "Accelerated insulation aging due to fast, repetitive voltages: A review identifying challenges and future research needs," *IEEE Trans. Dielectr. Electr. Insul.*, vol. 26, no. 5, pp. 1558–1568, Oct. 2019.
- [4] B. Zhang *et al.*, "Electrical Properties of Silicone Gel for WBG-Based Power Module Packaging at High Temperatures," *IEEE Trans. Dielectr. Electr. Insul.*, vol. 30, no. 2, pp. 852–861, Apr. 2023.
- [5] B. Zhang et al., "Dielectric Properties Characterization and Evaluation of Commercial Silicone Gels for High-Voltage High-Power Power Electronics Module Packaging," *IEEE Trans. Dielectr. Electr. Insul.*, vol. 30, no. 1, pp. 210–219, Feb. 2023.
- [6] M. Borghei, M. Ghassemi, "A Finite Element Analysis Model for Partial Discharges in Silicone Gel under a High Slew Rate, High-Frequency Square Wave Voltage in Low-Pressure Conditions," *Energies*, vol. 13, p. 2152, 2020.
- [7] M. M. Tousi and M. Ghassemi, "The effect of type of voltage (sinusoidal and square waveform) and the frequency on the performance of nonlinear field-dependent conductivity coatings for electric field control in power electronic modules," *IEEE Conf. Electrical Insulation and Dielectric Phenomena (CEIDP)*, Richland, 2019, pp. 552–555.
- [8] P. Adhikari and M. Ghassemi, "A Review of Insulation Challenges and Mitigation Strategies in (U)WBG Power Modules Packaging," *IEEE Texas Power* and *Energy Conference (TPEC)*, College Station, TX, USA, 2024.
- [9] M. M. Tousi and M. Ghassemi, "Nonlinear field dependent conductivity materials for electric field control within next-generation wide bandgap power electronics modules," *IEEE Electrical Insulation Conference* (EIC), 2019, pp. 63–66.
- [10] M. M. Tousi and M. Ghassemi, "Electric field control by nonlinear field dependent conductivity dielectrics characterization for high voltage

- power module packaging," *IEEE International Workshop on Integrated Power Packaging (IWIPP)*, Toulouse, France, 2019, pp. 54–58.
- [11] M. M. Tousi and M. Ghassemi, "Electrical insulation packaging for a 20 kV high density wide bandgap power module," *IEEE Energy Conversion Congress and Exposition (ECCE)*, 2019, pp. 4162–4166.
- [12] F. Yan, L. Wang, Y. Gan, K. Li, and B. Zhang, "A New Structure of Ceramic Substrate to Reduce the Critical Electric Field in High Voltage Power Modules," *J. Electron. Packag.*, vol. 144, Feb. 2022.
- [13] L. Zhong et al., "An Integrated Structure–Material Optimization Strategy for the Packaging of High-Voltage Insulated Gate Bipolar Transistors," *IEEE Trans. Dielectr. Electr. Insul.*, vol. 29, no. 6, pp. 2163–2170, Dec. 2022.
- [14] Y. Wang, J. Wu, Y. Yin, and T. Han, "Effect of micro and nano-size boron nitride and silicon carbide on thermal properties and partial discharge resistance of silicone elastomer composite," *IEEE Trans. Dielectr. Electr. Insul.*, vol. 27, no. 2, pp. 377–385, Apr. 2020.
- [15] S. Diaham, Z. Valdez-Nava, T. T. Le, L. Lévêque, L. Laudebat, and T. Lebey, "Field Grading Composites Tailored by Electrophoresis—Part 2: Permittivity Gradient in Non-Uniform Electric Field," *IEEE Trans. Dielectr. Electr. Insul.*, vol. 28, no. 2, pp. 341–347, Apr. 2021.
- [16] H. Yao et al., "Two-Stage Electric Field Optimization Method for High-Voltage Power Module Using Dielectrically Graded Insulation Micro-Region," *IEEE Trans. Dielectr. Electr. Insul.*, vol. 30, no. 3, pp. 1005–1015, Jun. 2023.
- [17] H. Gao and P. Liu, "High-Temperature Encapsulation Materials for Power Modules: Technology and Future Development Trends," *IEEE Trans. Compon. Packag. Manuf. Technol.*, vol. 12, no. 11, pp. 1867–1881, Nov. 2022.
- [18] M. M. Tousi and M. Ghassemi, "Combined geometrical techniques and applying nonlinear field dependent conductivity layers to address the high electric field stress issue in high voltage high-density wide bandgap power modules," *IEEE Trans. Dielectr. Electr. Insul.*, vol. 27, no. 1, pp. 305–313, Feb. 2020.
- [19] K. Li, B. Zhang, X. Li, F. Yan, and L. Wang, "Electric Field Mitigation in High-Voltage High-Power IGBT Modules Using Nonlinear Conductivity Composites," *IEEE Trans. Compon. Packag. Manuf. Technol.*, vol. 11, no. 11, pp. 1844–1855, Nov. 2021.
- [20] K.-B. Sun, Y.-H. Mei, Z.-B. Shuai, and L. Li, "Insulation and Reliability Enhancement by a Nonlinear Conductive Polymer-Nanoparticle Coating for Packaging of High-Voltage Power Devices," *IEEE Trans. Dielectr. Electr. Insul.*, pp. 1–1, 2023
- [21] M. M. Tousi and M. Ghassemi, "Effects of Frequency and Temperature on Electric Field Mitigation Method via Protruding Substrate Combined with Applying Nonlinear FDC Layer in Wide Bandgap Power Modules," *Energies*, vol. 13, no. 8, Jan. 2020.
- [22] M. Ghassemi, "PD measurements, failure analysis, and control in high-power IGBT modules," *High Volt.*, vol. 3, no. 3, pp. 170–178, 2018.
- [23] H. Reynes, C. Buttay, and H. Morel, "Protruding ceramic substrates for high voltage packaging of wide bandgap semiconductors," *IEEE Workshop on Wide Bandgap Power Devices and Applications (WiPDA)*, Oct. 2017, pp. 404–410.
- [24] M. M. Tousi and M. Ghassemi, "Characterization of Nonlinear Field-Dependent Conductivity Layer Coupled With Protruding Substrate to Address High Electric Field Issue Within High-Voltage High-Density Wide Bandgap Power Modules," *IEEE J. Emerg. Sel. Top. Power Electron.*, vol. 8, no. 1, pp. 343–350, Mar. 2020.
- [25] M.-R. Halloum, B. S. Reddy, and G. N. Reddy, "Stress Control for Polymeric Outdoor Insulators Using Nonlinear Resistive Field Grading Materials Operating Under Different Conditions," *IEEE Trans. Dielectr. Electr. Insul.*, vol. 29, no. 3, pp. 1175–1182, Jun. 2022.
- [26] M. M. Tousi and M. Ghassemi, "Nonlinear Resistive Electric Field Grading in High-Voltage, High-Power Wide Bandgap Power Module Packaging," *IEEE Energy Convers. Congr. & Expo. (ECCE)*, Sep. 2019, pp. 7124–7129.